Optimization of Satellite Antenna Placement at a Ground Control Station using UAV LiDAR Data

Patryk Wróblewski, Anna Fryśkowska-Skibniewska, Paulina Jaczewska

Faculty of Civil Engineering and Geodesy, Military University of Technology, gen. Sylwestra Kaliskiego 2, 00-908 Warsaw, Poland

patryk.wroblewski@wat.edu.pl, anna.fryskowska@wat.edu.pl, paulina.jaczewska@wat.edu.pl

Keywords: Point Cloud, LiDAR, UAV, Elevation Mask, Satellite Mission Planning, Visibility Analysis

Abstract

Reliable communication between satellites and ground control stations (GCS) is fundamental to modern space missions, with its effectiveness being directly dependent on an unobstructed Line-of-Sight (LoS). Traditional site planning methods, relying on low-resolution terrain models, often overlook crucial obstacles like buildings or dense vegetation. This paper presents a comprehensive methodology using high-resolution Light Detection and Ranging (LiDAR) data, acquired from an Unmanned Aerial Vehicle (UAV), to precisely model horizon obstruction and optimize the placement of transceiver antennas. The methodology was verified on a real-world case study in Zielona Góra, Poland. The workflow included data acquisition, PPK-based trajectory processing, and point cloud subsampling using an Octree-based algorithm. The core of this work was the implementation of an algorithm to generate detailed elevation masks by calculating the maximum obstruction angle for defined azimuthal intervals. The analysis clearly identified the superior of two potential locations, proving the method's effectiveness as a decision-support tool in the space sector.

1. Introduction

The dynamic growth of the space sector, particularly the increasing number of satellite missions, generates a demand for effective and reliable communication between objects in orbit and Ground Stations. A key factor determining the quality and duration of this communication is an unobstructed Line-of-Sight (LoS) between the transceiver antenna and the satellite. Terrain obstacles and land cover features, both natural and anthropogenic, can significantly limit the radio horizon, shortening communication windows and affecting connection stability.

Traditional methods for assessing ground station locations often rely on global, low-resolution Digital Terrain Models (DTMs), which do not account for land cover objects such as buildings or tall vegetation. While Digital Surface Models (DSMs) offer a significant improvement by including the elevation of such features, they still represent the environment as a 2.5D grid. This limitation prevents DSMs from fully capturing complex, fully 3D structures like overhanging vegetation branches or open-lattice telecommunication masts, which can partially obstruct the Line-of-Sight. Therefore, raw 3D point clouds provide the most comprehensive spatial representation. The development of remote sensing technologies, especially Airborne Laser Scanning (ALS) from manned and unmanned (UAV) platforms, opens up new possibilities for precise three-dimensional space modeling (Guimarães et al., 2020). Data in the form of a dense LiDAR point cloud allows for the creation of highly detailed horizon obstruction models, known as elevation masks.

The aim of this paper is to present a complete methodology for selecting the optimal location for a ground station antenna based on LiDAR data acquired using an Unmanned Aerial Vehicle (UAV). The paper presents the entire process, from mission planning and data acquisition, through processing, to the generation and analysis of elevation masks for various location and height variants. The study was conducted for a real-world site located in Zielona Góra, Poland. Consequently, this study aims to address the following research questions: (1) Does high-resolution UAV-LiDAR data significantly alter the calculated horizon obstruction compared to generalized spatial data? (2) To what extent does the angular resolution of the elevation mask impact the representation of narrow obstacles? Therefore, the hypotheses are that standard spatial datasets underestimate horizon masking in dynamic urban environments (H1), and that fine angular intervals ($\leq 0.5°$) are necessary to reliably model local obstructions without overgeneralizing (H2).

2. Related Work

Reliable telemetry, tracking, and command (TT&C) operations between satellites and Ground Control Stations (GCS) strictly depend on an unobstructed Line-of-Sight (LoS). Traditional methodologies for determining GCS locations and calculating horizon obstruction have heavily relied on 2.5D raster datasets. While early approaches utilized global Digital Terrain Models (DTMs) that ignore surface objects, more recent GIS-based viewshed analyses have adopted Digital Surface Models (DSMs). However, as noted in recent spatial studies, 2.5D models often overgeneralize complex 3D environments, failing to accurately represent structures like open-lattice towers or overhanging canopy branches.

In recent years, high-density point clouds acquired via UAV-LiDAR have emerged as the standard for precise 3D environment modeling (Guimarães et al., 2020). While the usage of UAV-LiDAR is well-documented, its explicit integration into satellite mission planning remains sparse. Furthermore, processing massive LiDAR datasets requires computationally efficient downsampling, with Octree-based algorithms proving highly effective at preserving critical structural geometry (Girardeau-Montaut, 2022). Ensuring trajectory accuracy is also vital, where Post-Processing Kinematic (PPK) methods have been shown to provide more robust results than real-time (RTK) approaches in challenging environments (Tomaštík et al., 2019). Existing methodologies often require manual processing or lack automated conversion into standardized aerospace formats. This paper bridges that gap by proposing an optimized workflow that directly utilizes dense 3D point clouds to compute precise elevation masks, bypassing the limitations of 2.5D viewshed algorithms.

3. Study Area and Data

3.1 Study Area Description

The analyzed area is located in the city of Zielona Góra (Nowy Kisielin district, Lubuskie Voivodeship), in the southwestern part of Poland. This area is characterized by varied topography and land cover, including both urbanized zones (industrial and residential buildings) and forested areas with significant elevation differences. This characteristic makes precise determination of horizon obstruction crucial for the success of the analysis. A specific cadastral parcel was selected for detailed study, within which two potential locations for the transceiver antenna (#1 and #2) were considered, as shown in Figure 1. Due to the terrain's topography, a 482-hectare buffer zone around the designated parcel was included in the analysis (Figure 2).

Figure 1. The analysed cadastral parcel (outlined with a red dashed line) with the two considered antenna locations (indicated #1 and #2).

Figure 2. The extended area covered by the analysis (yellow dashed line). The specific cadastral parcel from Figure 1 is highlighted in the center with a red dashed line.

3.2 Geospatial Data Acquisition

To obtain high-resolution 3D data, a photogrammetric flight was conducted in May 2025 using a DJI Matrice 300 RTK UAV equipped with an integrated Zenmuse L1 laser scanner. A crucial first step was the decision to acquire new data rather than relying on existing, publicly available resources. While some countries, including Poland, provide nationwide LiDAR datasets, their suitability for this specific, high-precision analysis is questionable for several reasons. Firstly, data currency is a critical factor, as the presence of new obstacles (e.g., recent construction, vegetation growth) can completely alter visibility conditions. Public datasets in Poland exhibit varied timeliness, with approximately 50% of the country covered by data from before 2023, and only smaller portions updated in 2023 (20%), 2024 (20%), and 2025 (10%). Secondly, the spatial resolution of these datasets is inconsistent, ranging from 4 to 25 pts/m², with an average of 10-12 pts/m². This resolution may be insufficient to capture fine-detailed obstacles like narrow masts, power lines, or individual tree branches that can significantly impact LoS. Finally, the processing methodology of publicly available data is often a "black box", meaning that crucial information may have been lost during pre-processing steps like downsampling before public release. Given these limitations, acquiring a dedicated, up-to-date, and high-resolution dataset was deemed essential for the reliability of the study.

Mission planning, performed using DJI Pilot software as shown in Figure 3 , is a critical stage that influences the quality of the final product and the efficiency of the entire workflow (Padró et al., 2019).

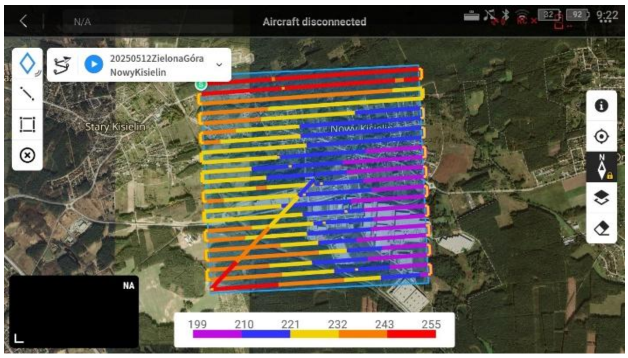

Figure 3. Mission plan in the DJI Pilot application.

The selection of flight parameters was a deliberate process aimed at optimizing the balance between data quality, acquisition time, and operational safety.

1. **Flight Altitude** (105 m AGL): This altitude was chosen as an optimal compromise. Flying lower (e.g., 50 m AGL) would have drastically increased the data acquisition time and generated an unnecessarily dense point cloud (well over 100 pts/m²), which would later be downsampled anyway. Flying higher would have shortened the flight time, but was constrained by two factors: Polish aviation law, which limits UAV flights to 120 m AGL, and the significant terrain elevation changes within the study area. The mission was executed in "Terrain Follow" mode, relying on the ASTER Global Digital Elevation Model (ASTER GDEM v3) (Abrams, Crippen, & Fujisada, 2020). Due to potential inaccuracies or outdated information in this global DEM, a conservative safety buffer of 15 m was applied, resulting in the final flight altitude of 105 m AGL. This approach ensured both safety and the acquisition of a point cloud with a density of approximately 65 pts/m², which is more than sufficient for the analysis.
2. **Flight Speed** (12 m/s): This speed was selected as it was the maximum permissible value for the other mission parameters (altitude, scan mode, etc.). A

higher speed contributes to optimizing the mission time by reducing the overall flight duration, while still achieving the target point density.

3. **Sidelap** (20%): A minimal sidelap of 20% was used. This value is sufficient to ensure the geometric integrity of the data block, which is necessary for the subsequent strip adjustment process. Increasing the side-lap would have unnecessarily increased flight time and data volume without providing significant benefits for this application, especially considering that a downsampling step was planned.
4. **Scan Mode and Returns:** The "Non-repetitive" scanning mode, which creates an elliptical, rotational scan pattern, was chosen over the linear "Repetitive" mode. This, combined with the registration of up to three laser beam returns, was intended to maximize vegetation penetration and provide a more complete and detailed 3D representation of all objects, including the ground surface beneath the canopy.

Concurrently, RGB images were acquired, which were used to colorize the point cloud, facilitating its visual interpretation.

4. Methodology

The proposed methodology presents a complete and highly optimized workflow for generating precise elevation masks from UAV-LiDAR data. A key innovation of this approach lies in its comprehensiveness and potential for automation, addressing the shortcomings of existing solutions. Currently, no single software package offers a complete toolset for such an analysis. While open-source programs like CloudCompare provide powerful tools for individual steps (Girardeau-Montaut, 2022), they lack a unified workflow, often requiring manual data selection and subjective parameter tuning. Furthermore, automation capabilities are either limited to internal toolsets (e.g., CloudCompare's command-line interface) or are in early, experimental stages. For instance, the Python plugin for CloudCompare is officially described as being in a "very early stage," limiting its reliability for production workflows.

Our approach overcomes these limitations by integrating an optimized field acquisition strategy with a computationally efficient data processing pipeline. This allows for the rapid survey of large areas and swift delivery of final results, including the elevation mask in the industry-standard “.aem” format, ready for direct use in mission planning software like Systems Tool Kit (STK). The entire workflow is structured into six main stages, as described below.

1. **Preliminary Area Analysis**: The first, manual step involves analyzing the terrain surrounding the potential antenna sites using publicly available data sources (e.g., global DEMs). This analysis aims to delineate the minimum required area for the field survey, ensuring that all potentially obstructing terrain features and objects were included within the flight plan's boundaries. This step prevents the unnecessary acquisition of data for areas that have no impact on the final result, thus optimizing the scope of fieldwork.
2. **Mission Planning**: Based on the delineated area, a detailed flight plan is created, with parameters chosen to optimize data quality and acquisition efficiency, as described in Section 2.2.
3. **Data Acquisition**: The UAV flight is executed to collect the raw LiDAR and RGB data.
4. **Data preprocessing**: This multi-step phase aims to produce a clean, georeferenced, and computationally efficient point cloud.
    a. **Trajectory Enhancement**: RINEX observation files are acquired from nearby permanent reference stations. These files are used to replace the original rover observation files (“.RTB” format from the Zenmuse L1), enabling a more accurate trajectory calculation.
    b. **PPK Processing**: The UAV's trajectory is computed in Post-Processing Kinematic (PPK) mode using DJI Terra software. PPK is generally considered more robust and capable of achieving higher accuracy than real-time kinematic (RTK) methods, as it allows for more advanced processing algorithms and does not depend on a continuous radio link (Tomaštík et al., 2019).
    c. **Strip Adjustment**: To minimize residual errors from the Inertial Measurement Unit (IMU), a strip adjustment is performed in OPALS software using the trajectory (“_sbet.out”) and point cloud exported from DJI Terra. This process ensures high geometric consistency between adjacent flight lines.
    d. **Point Cloud Downsampling**: The final step is downsampling the dense point cloud to optimize the performance of subsequent computational tasks. The Octree-based method is chosen. Unlike simpler methods like random or spatial subsampling, the Octree structure recursively subdivides the 3D space, preserving points in areas of high geometric complexity. This ensures that critical features like building edges, ridgelines, and treetops are retained, while reducing point density in flat, homogenous areas (Girardeau-Montaut, 2022). This targeted reduction is key to minimizing processing time without sacrificing essential details.
5. **Core Data Processing**: For each potential location and antenna height, the core algorithm for elevation mask generation is executed. The detailed logic of this step is formalized mathematically in the subsequent section.
6. **Results Analysis and Selection**: The generated elevation masks are analyzed to select the optimal antenna location and mounting height. This involves comparing the visibility at heights of 1.5 m, 10 m, 15 m, and 20 m AGL. The 1.5 m height represents a ground-level installation, while the subsequent 5-meter intervals up to 20 m (a height exceeding the tallest local structures) are chosen to evaluate the trade-off between improved visibility and the increased cost of constructing a taller mast. The analysis also considered the impact of the mask's angular resolution, confirming that a finer interval provides a more reliable representation of the horizon.

4.1 Data Pre-processing

The raw data undergoes a processing workflow to obtain a georeferentially accurate and noise-free point cloud. The UAV flight trajectory is determined in Post-Processing Kinematic (PPK) mode using DJI Terra software and observation data from

https://doi.org/10.5194/isprs-archives-XLIX-B4-2026-275-2026 |

national reference stations network. To further minimize Inertial Navigation System (INS) errors, a final strip adjustment is performed in the specialized scientific software OPALS, using the exported “_sbet.out” trajectory (Pfeifer et al., 2014).

The initial data processing takes approximately 8 hours and is performed on a high-performance virtual machine; its hardware specifications are detailed in Table 1.

Component	Specification
CPU	Intel(R) Xeon(R) Gold 6348 CPU @ 2.60GHz
GPU	2 x NVIDIA A100 80 GB
RAM	256 GB
Disk	2.00 TB SSD VMware Virtual disk, 20.00 TB HDD VMware Virtual disk
OS	Windows 10 Education, 64-bit

Table 1. Hardware specifications of the workstation used for data processing.

The resulting point cloud, consisting of approximately 785 million points, is subjected to further operations. First, a statistical outlier removal filter is applied to eliminate noise that could negatively affect subsequent analyses. Then, to optimize computations, the point cloud is downsampled. An Octree-based method is used, which effectively reduces the number of points while preserving key geometric features of the terrain and objects (Girardeau-Montaut, 2022). This process reduces the number of points to about 3 million, significantly shortening the time for further analysis while maintaining the necessary level of detail (Figure 4).

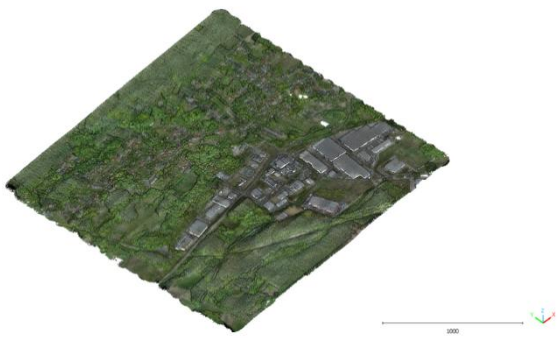

Figure 4. The final point cloud prepared for analysis, thinned using an Octree-based method.

4.2 Elevation Mask Generation

The core of the analysis is the generation of elevation masks for each considered location and antenna mounting height (1.5 m, 10 m, 15 m, 20 m AGL). The core logic of the elevation mask generation is formalized mathematically. For a given antenna location $L = (x_{ant}, y_{ant}, z_{ant})$ where z_{ant} includes the mounting height above ground level, the required elevation angle θ_i for each valid point $P_i = (x_i, y_i, z_i)$ in the point cloud where $z_i \geq z_{ant}$ is calculated as:

$$\theta_i = \arctan\left(\frac{z_i - z_{ant}}{\sqrt{(x_i - x_{ant})^2 + (y_i - y_{ant})^2}}\right) \tag{1}$$

The corresponding azimuth angle α_i is similarly derived. To discretize the horizon, the azimuthal space $(0° - 360°)$ is divided into equal bins of a defined angular interval $\Delta\alpha$ (e.g., 0.5°). The final elevation mask value M_k for a given azimuth bin k is obtained by applying the maximum function:

$$M_k = \max_{i \in S_k}(\theta_i) \tag{2}$$

where S_k is the subset of all points P_i whose azimuth α_i falls within the k-th bin. If a bin contains no points, the mask defaults to $-90°$. This formally defines the computational complexity of the mask generation algorithm as $O(N)$, relative to the number of points N.

This approach is a form of "viewshed" analysis, commonly used in GIS, but here it is implemented directly on the irregular data structure of a point cloud (Floriani and Magillo, 2003). A visualization of the point cloud, where the attribute is the calculated elevation angle, is shown in Figure 5.

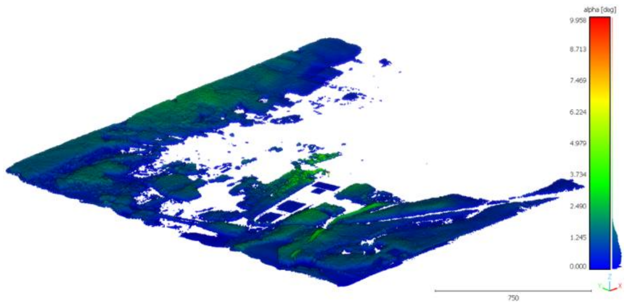

Figure 5. Point cloud with an attribute representing the elevation of points above the horizon plane (expressed in degrees).

The final output is not only a graphical representation but also a data file in the Azimuth-Elevation Mask (“.aem”) format, a standard for professional space mission simulation software like AGI's Systems Tool Kit (STK). This ensures the direct applicability of the results in an engineering workflow. The conversion from an internal .csv format to the final .aem file is performed by a dedicated automated script.

5. Results and Discussion

As a result of applying the described methodology, elevation masks were generated for each combination of antenna location and height. Sample visualizations in the form of radar and line charts for a height of 15 m AGL are presented in Figures 6 and 7. To aid in the interpretation of these results, panoramic images were also generated, providing real-world visual context for the quantitative data, as shown in Figure 8 for location #1.

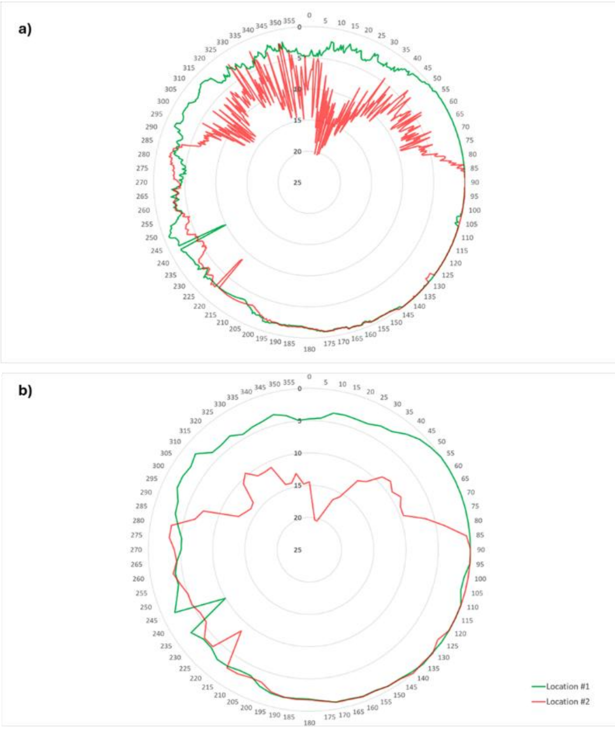

Figure 6. Examples of elevation mask visualization as a radar plot for both analyzed locations and a planned antenna height of 15 m AGL. Note how the finer 0.5° resolution (a) accurately captures narrow structures like individual trees or masts, which are overly smoothed and generalized in the 5° resolution (b).

Figure 7. Examples of elevation mask visualization as a line plot for both analyzed locations and a planned antenna height of 15 m AGL. Similarly to the radar plot, the 0.5° angular interval (a) provides a much more faithful representation of actual obstacles compared to the generalized 5° interval (b).

Figure 8. A panoramic image generated from photos taken at location #1 at a height of 15 m AGL.

The analysis of the results clearly shows that location #1 offers significantly better visibility conditions, especially in key azimuthal sectors. The horizon for location #2 is largely obstructed by nearby buildings and tall vegetation, resulting in elevation values reaching up to 20°.

A key element of the discussion is the impact of algorithm parameters on the final result. A comparison of masks generated with angular intervals of 0.5° and 5° (Figures 6 and 7) shows that a smaller interval allows for a much more faithful representation of actual obstacles. Wide intervals, although they smooth the graph, can lead to generalizations, such as extending the influence of a single, narrow object (like a mast) over an entire azimuthal sector. Given that Octree-based downsampling already optimized the dataset at an early stage, using small intervals (e.g., 0.5°) is recommended to achieve maximum reliability.

Equally important is the choice of the statistical function for aggregating values within the azimuthal bins. The comparison of MAX and MEAN functions (Figure 9) clearly indicates that MAX is the correct approach, ensuring that the highest obstacle in a given sector is considered. The MEAN function averages the values, leading to a drastic underestimation of the real horizon obstruction and could result in flawed design conclusions.

Figure 9. The difference between the elevation mask generated using the MAX and MEAN functions for location #1 and an antenna height of 15 m AGL.

5.1 Innovation and Research Potential

The proposed methodology provides a solid foundation that can be further developed. An interesting direction would be the implementation of point cloud semantic segmentation algorithms using deep learning (e.g., RandLA-Net or KPConv networks). This would allow for the distinction between types of obstacles (e.g., buildings vs. vegetation). Such information could be used to model signal propagation for different frequencies, as radio signals interact differently with various types of objects (Guo et al., 2020).

6. Conclusions

This paper presented and verified a complete methodology for using UAV-LiDAR data for the precise determination of horizon obstruction masks for the purpose of optimizing the location of satellite mission ground control stations. The analyses showed that:

1. UAV-LiDAR technology is a highly effective tool for acquiring detailed 3D data for visibility analyses in complex terrain.
2. The use of an Octree-based downsampling method allows for significant data reduction while preserving key information about the terrain's relief and land cover.
3. The choice of elevation mask generation parameters, such as the angular interval and statistical function, has a critical impact on the reliability of the results. It is recommended to use small intervals ($\leq 0.5°$) and the MAX function to ensure all potential obstacles are accounted for.
4. The presented methodology can be successfully applied in engineering practice to support decision-making processes in the space industry, minimizing risks and optimizing costs associated with the construction of ground infrastructure.

Further research could focus on automating the process and integrating the results with space mission simulation software, as well as enriching the analysis with semantic segmentation of obstructing objects.

References

Abrams, M., Crippen, R., Fujisada, H., 2020. ASTER Global Digital Elevation Model (GDEM) and ASTER Global Water Body Database (ASTWBD). *Remote Sensing, 12(7), 1156.*

Floriani, L. D., Magillo, P., 2003. Algorithms for visibility computation on terrains: a survey. *Environment and Planning B: Planning and Design, 30(5), 709-728.*

Girardeau-Montaut, D., 2022. CloudCompare (version 2.12) [GPL software]. Retrieved from http://www.cloudcompare.org/

Guimarães, N., Pádua, L., Marques, P., Silva, N., Peres, E., Sousa, J. J., 2020. Forestry remote sensing from unmanned aerial vehicles: A review focusing on the data, processing and potentialities. *Remote Sensing*, 12(6), 1046.

Guo, Y., Wang, H., Hu, Q., Liu, H., Liu, L., Bennamoun, M., 2020. Deep learning for 3d point clouds: A survey. *IEEE Transactions on Pattern Analysis and Machine Intelligence, 43(12), 4338-4364.*

Padró, J. C., Muñoz, F. J., Planas, J., Pons, X., 2019. Comparison of four UAV georeferencing methods for environmental monitoring purposes focusing on the combined use with airborne and satellite remote sensing platforms. *International Journal of Applied Earth Observation and Geoinformation*, 75, 130-140.

Pfeifer, N., Mandlburger, G., Otepka, J., Karel, W., 2014. OPALS - A framework for Airborne Laser Scanning data analysis. *Computers, Environment and Urban Systems, 45, 125-136.*

Tomaštík, J., Mokroš, M., Surový, P., Grznárová, A., Merganič, J., 2019. UAV RTK/PPK Method—An Optimal Solution for Mapping Inaccessible Forested Areas? *Remote Sensing*, 11(6), 721.